Electronic and atomic structure of a dissociated dislocation in $SrTiO_3$

Zaoli Zhang, Wilfried Sigle, Wolfgang Kurtz, and Manfred Rühle
Max-Planck-Institut für Metallforschung, Heisenbergstraße 3, D-70569 Stuttgart, Germany
(Received 29 July 2002; published 31 December 2002)

A [001](110) small-angle grain boundary $SrTiO_3$ was studied by electron-energy-loss spectroscopy (EELS) and high-resolution transmission electron microscopy. The $a\langle 110\rangle$ grain boundary dislocations were dissociated into two partial dislocations involving climb of the partials. From their separation an upper limit of the (110) antiphase boundary energy of (720 ± 280) mJ/m^2 is deduced. EELS spectra were obtained from the partial cores and the antiphase boundary in a dedicated scanning transmission electron microscope. The Sr/Ti ratio was found to be increased in one of the partial cores but decreased in the other. This can be understood from the dissociation mechanism. From the increase of the Ti/O ratio it is concluded that the dislocation cores are oxygen deficient. Ti-$L_{2,3}$ EELS spectra show a reduction of Ti in the partial dislocation cores as well as a reduced crystal field. Atomic models of the dissociated dislocation cores are established.

DOI: 10.1103/PhysRevB.66.214112 PACS number(s): 61.72.Mm, 82.80.Pv, 61.72.Ff

I. INTRODUCTION

Grain boundaries (GBs) are known to have a dominant effect on the macroscopic electric properties of oxides. In the perovskite oxides $ATiO_3$ (A=Sr, Ca, Ba), GBs often provide the prerequisite for technological applications.[1] Recently, the atomic structure and electronic properties of various special grain boundaries in $SrTiO_3$ have been studied.[1–14] It was suggested that the electrical properties of $SrTiO_3$ can be understood in terms of acceptor states at the grain boundary core.[15,16] The space charge associated with these charged states is assumed to form a barrier against the electronic and ionic transport. Thus the grain boundary structure and the bonding of atoms at the grain boundary dictate its electronic behavior. In the light of this, a knowledge of the structure and chemistry at the grain boundary is of fundamental importance. Recently efforts were made to combine *Z*-contrast imaging and electron-energy-loss spectroscopy (EELS) in order to provide the atomic-scale structure and composition at particular GB's in $SrTiO_3$ with sufficient high resolution.[8,9] By *ab initio* calculations and empirical simulations detailed information of the bonding of atoms was obtained on some special grain boundaries.[2,17,18] All these have also been demonstrated on the atomic and electronic structure of edge and dissociated dislocation core by EELS in some materials.[19,20]

The main focus of most previous studies was on the electronic and atomic structure of large angle grain boundaries. Recently it was shown that also low-angle tilt grain boundaries of $SrTiO_3$ can exhibit strong barriers for charge transport.[21] It is well known that such low-angle GB's are composed of isolated dislocations. For this reason we are presently studying the atomistic and electronic structure of dislocations in $SrTiO_3$. Owing to the one-dimensional geometry of dislocations the experimental determination of the electronic structure and chemistry is even more challenging than within GB's. Nonetheless this has been demonstrated recently in Si, GaN, and $SrTiO_3$.[19,20,22] Whereas in Ref. 22 we reported about the $a\langle 100\rangle$ edge dislocation in $SrTiO_3$, here we focus on EELS measurements and high-resolution transmission electron microscopy (HRTEM) characterization of a dissociated dislocation in a [001] (110) small angle tilt GB in $SrTiO_3$.

II. EXPERIMENTAL PROCEDURES

A $SrTiO_3$ bicrystal with an [001] (110) small angle tilt grain boundary of $\sim 5°$ tilt angle has been produced by diffusion bonding of two undoped $SrTiO_3$ crystal platelets (purchased from CRYSTAL GmbH, Berlin) in ultra high vacuum (UHV).[23,24] The polished surfaces to be bonded have been tilted by $\sim 2.5°$ around the $\langle 001\rangle$ axis (more precisely, 2.34° and 2.39°); in addition, there was also a tilt component around $\langle -1\ 1\ 0\rangle$ of 0.16° due to the miscut of the crystal surfaces). The crystals have been ultrasonically cleaned in propanone, sputter cleaned *in situ* using Ar^+ ions of about 1.3 keV energy. The sputtered surfaces have been exposed for less than half an hour to the UHV ambient (in the low 10^{-9}-Pa range) before being protected by the other crystal. The appropriately oriented crystal stack has been loaded with 1 MPa and heated within 2.5 h to 1450 °C at $\sim 10^{-7}$ Pa and kept there for 6 h then cooled down to room temperature within 2.5 h, always under an applied load of 1 MPa. Owing to the loss of oxygen during the bonding in UHV the final bicrystal was opaque. After a heat treatment in air at 1200 °C for 24 h the bicrystal transparency was regained. The cooling and heating rates were 5 °C per minute.

The TEM sample preparation procedure is as described in our former paper.[22] In addition a final ion polishing with low-energy Ar ions (0.5 keV) was done using a LINDA ion mill produced by TECHNOORG LINDA. A JEOL 4000EX microscope operated at 400 kV with a point resolution of 0.17 nm was used for high-resolution imaging. HRTEM phase contrast images were acquired parallel to the [001] zone axis which is common to both grains.

For analytical TEM a dedicated scanning transmission electron microscopy (VG HB 501 UX, Vacuum Generators) was used. The microscope was operated at 100 keV. It is equipped with a cold field-emission gun, an energy dispersive x-ray spectrometer (Noran) and an electron energy-loss spectrometer (Gatan UHV ENFINA 766). The energy resolution in EELS, as measured by the full width at half maxi-

 ©2002 The American Physical Society

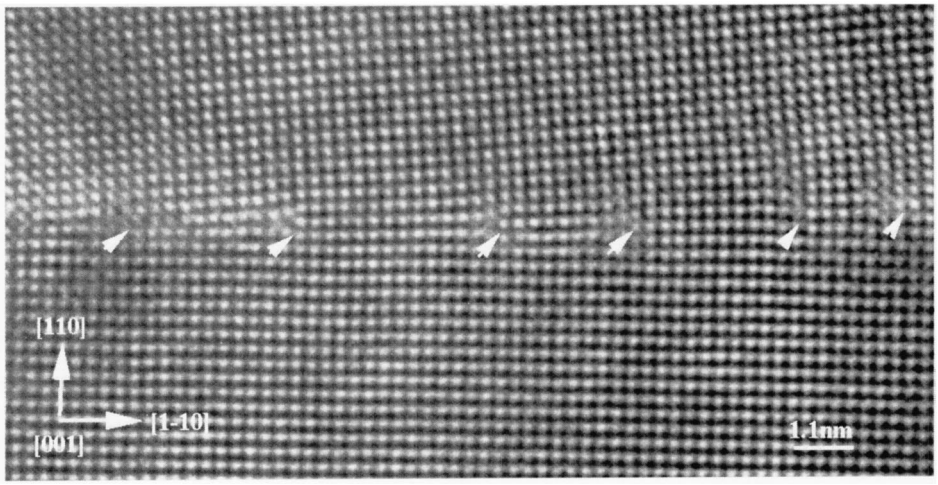

FIG. 1. HRTEM image of the 5° [001](110) symmetrical tilt grain boundary. Note that each GB dislocation has dissociated into two partial dislocations by a climb mechanism.

mum of the zero-loss peak, was 0.7 eV. At the microscope setting used, the electron probe size is smaller than 0.5 nm. However, due to the beam broadening in the specimen (thickness t) and the finite acceptance half-angle β of the spectrometer (6.5 mrad), the spatial resolution of our measurements [which can be approximated by the product of β and t (Ref. 25)] is typically between 0.5 and 1 nm. Spectra were recorded with a dispersion of 0.1 eV/channel, which allows to simultaneously acquire the Ti-$L_{2,3}$ edge and the O-K edge and to determine peak positions with high accuracy. For the acquisition of the Sr-$L_{2,3}$ edge at an energy loss of 1940 eV a dispersion of 0.7 eV/channel was used. The energy scale for the EELS spectra was calibrated by setting the first white line of the Ti-$L_{2,3}$ edge to 456 eV or the Sr-$L_{2,3}$ edge to 1940 eV. For this reason energy shifts stated below denote *relative* energy shifts. The convergence and collection semi-angles were both 6.5 mrad. All data shown here were corrected for dark current of the photodiode array and detector gain variation. The spectrum acquisition and processing were done with the Digital Micrograph 3.6 Spectrum Imaging and EL/P software. The background for each spectrum was subtracted by the fit of a power-law function to the pre-edge background.[25]

Local information from the dislocation core can be obtained directly by placing the electron beam in the center of the core. Owing to the difficulty to locate the very core precisely, we measured EELS spectra from a small area containing the dislocation core or by acquiring a set of spectra within a matrix containing an individual core. The latter technique allows us to obtain spectra from areas containing only few atom columns around the dislocation core.

III. RESULTS

A. HRTEM

Figure 1 shows a HRTEM image of the small-angle GB. Individual dislocation cores can be clearly distinguished (white arrows). Burgers circuits around the cores reveal that the Burgers vector is $a/2[110]$, i.e., the GB dislocations are dissociated into partial dislocation. From the image it can be seen that the partial dislocations are separated from one another not on the common slip plane, but *along the GB*. This can only be achieved by a climb mechanism. The climb plane is (110), i.e. the partials are separated by an antiphase boundary (APB) on the (110) plane. The average dissociation width between two partial cores is (2.5 ± 0.3) nm. The average spacing between the partial pairs is (6.6 ± 0.3) nm. Based on these values the real misorientation angle can be calculated to be 3.5° by the Frank formula.

B. EELS analysis

EELS spectra were obtained through area measurements and mapping techniques.

1. Area measurement

Ti-$L_{2,3}$ and O-K EELS spectra were recorded while scanning the beam over a rectangular area of 3×4 nm^2. This area contains a pair of partial dislocation cores. During this measurement, specimen drift can be corrected manually during the acquisition since the image and EELS spectra are recorded simultaneously. Spectra were recorded from the grain boundary region and from the nearby bulk on either side of the grain boundary with a dispersion of 0.1 eV/channel. The total acquisition time was 30 s for each spectrum.

The Ti-$L_{2,3}$ edge and the O-K edge are presented in Fig. 2(a). The most remarkable change in the GB spectrum is the ratio of the $e_g:t_{2g}$ intensities[26] which is reduced by 48.5 ±19 % compared with that in the bulk. An enlargement of Fig. 2(a) is shown in Fig. 2(b). The dotted lines indicate the peak positions for the bulk spectrum. Compared to this, the crystal-field splitting in the GB spectrum is reduced by 0.1–0.2 eV. The quantification of these two peaks shows an increase of the Ti/O ratio by 3.2 ± 5.7% and of the L_3/L_2 ratio by 21 ± 3.5% compared with that in the bulk. The data analysis followed the techniques shown in[27] and using a Gaussian fitting method. Figure 2(c) presents the enlargement of the O-K edge. The second peak is slightly decreased compared with the spectrum from the bulk although the signal-noise ratio is low.

The composition of every pair of partial cores was measured by area measurements. Since the energy positions of

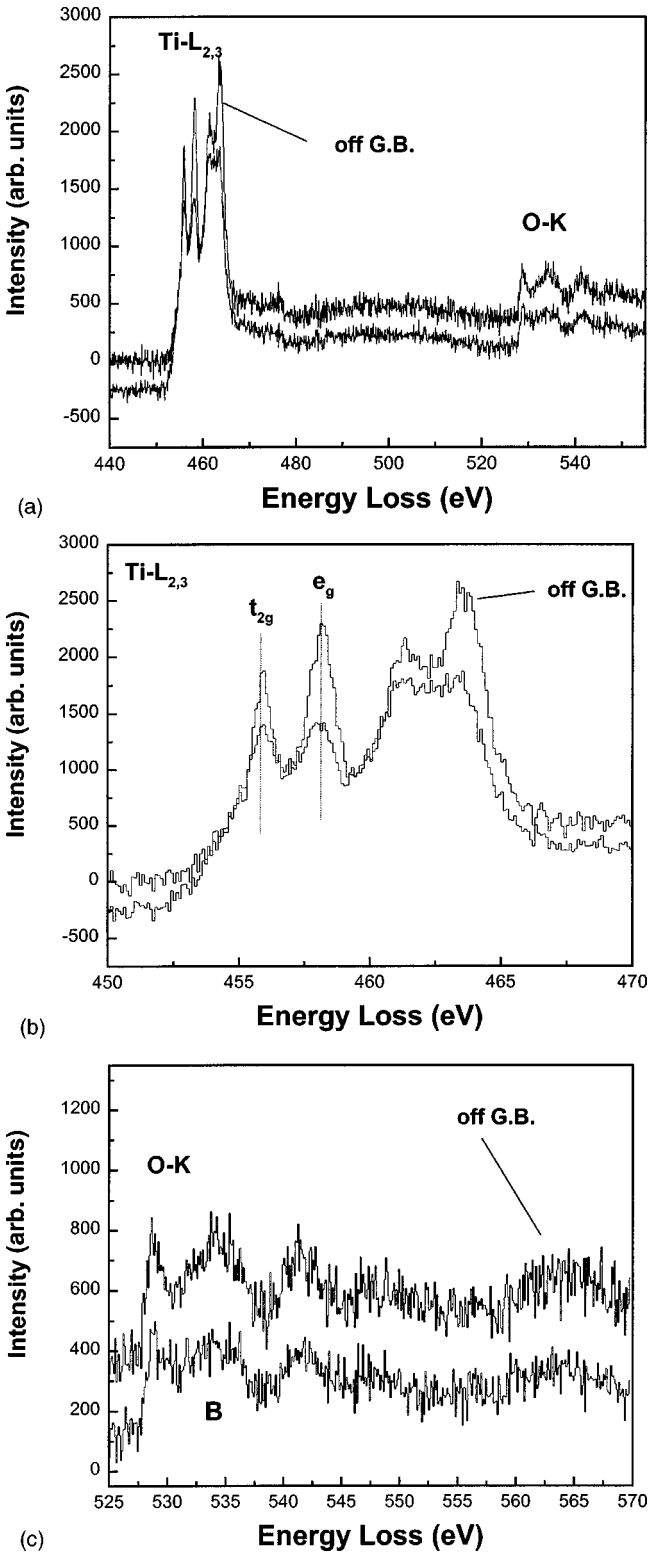

FIG. 2. (a) EELS spectrum from a 3×4 nm area containing a pair of partial dislocation cores. (b) Enlargement of the Ti-$L_{2,3}$ edge showing a decrease of the crystal-field splitting and the e_g/t_{2g} intensity ratio. (c) Enlargement of the O-*K* edge showing a decrease of peak *B*.

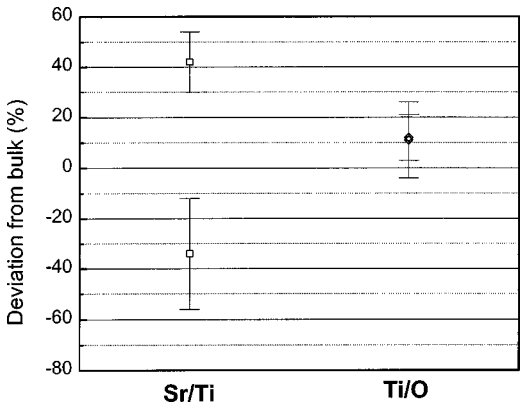

FIG. 3. The composition (Si/Ti and Ti/O ratios) of several pairs of partial dislocation cores obtained by the area measurement method.

the Ti-$L_{2,3}$, O-*K*, and Sr-$L_{2,3}$ edges are quite different, their spectra could not be recorded simultaneously. Therefore, the spectra were recorded separately using a dispersion of 0.3 eV/channel for the Ti-$L_{2,3}$ and O-*K* edges and one of 0.7 eV/channel for the Sr-$L_{2,3}$ edge. The total acquisition times for the Sr and Ti and O-*K* edges are 20 and 15 s respectively. Spectra from ten pairs of partial cores were recorded. The analysis followed the techniques shown in Ref. 25. It turned out that the chemical composition of the partials shows a bimodal distribution with a set of Sr deficient cores and a set of Sr-rich cores. Figure 3 shows the average composition from both sets. It can be seen that in both core types the Ti/O ratio is higher than in bulk, whereas the Sr/Ti ratio shows an increase in one core and a decrease in the other core.

2. EELS mapping

To make use of the high spatially resolved EELS in the STEM, nine EELS spectra (3×3) were recorded from a quadratic area (1.91×1.91 nm^2) containing one individual partial dislocation core. Thus the separation between neighboring measurements was about 0.6 nm. The integration time for each spectrum was 2 s. For most maps specimen drift was found to be much smaller than the pixel size. The spectrometer dispersion was 0.1 eV/channel. In general one or two spectra were found to be different from the others, and we then assigned this/these as the dislocation core specific spectrum/spectra. Figure 4(a) shows the Ti-$L_{2,3}$ and O-*K* spectra from one individual partial dislocation core and from the nearby bulk. The e_g and t_{2g} peaks are no longer visible as separate peaks [Fig. 4(b)] and the L_3/L_2 ratio is increased by $35\pm2\%$. The intensity of the second peak of the O-*K* edge is reduced in the core. An increase of the Ti/O ratio by $54\pm10\%$ in the core as compared to the bulk is found.

EELS spectra were obtained also from the APB. A line scan was performed across the APB with a total of ten spectra over a total length of 4.84 nm. The spectra were recorded using a dispersion of 0.1 eV and total acquisition time of 30 s. Figure 5 shows a comparison of the APB spectrum with an average bulk spectrum. The latter was obtained by adding seven bulk spectra. The crystal-field splitting is reduced by 0.3 ± 0.1 eV (it is more easily seen from the two smoothed

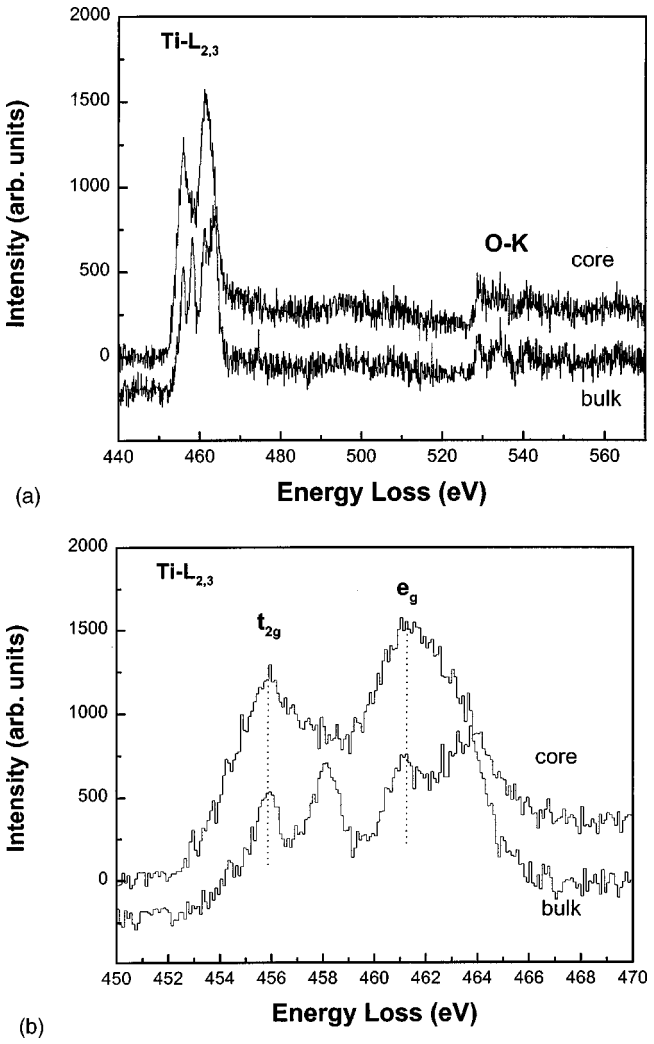

FIG. 4. (a) Two spectra extracted from the EELS map, one in a partial dislocation core and the other from the surrounding bulk region. (b) Enlargement of the Ti-$L_{2,3}$ edge showing a significant decrease of two e_g peaks.

spectra which were obtained with a 0.8 eV low-pass filter). No obvious change in the O-*K* edge was found since the spectrum was too noisy due to the short acquisition time.

IV. DISCUSSION

The Volterra construction of the $a[110]$ edge dislocation in $SrTiO_3$ is shown in Fig. 6(a). For this construction anisotropic elasticity is taken into account, and we assumed that the core has zero net charge. Due to the long Burgers vector four atom planes are inserted which terminate on the same $[1\bar{1}0]$ crystal plane. The inserted planes contain either only oxygen atoms or Ti, O, and Sr atoms. The mixed planes are terminated in the core by Sr or Ti/O columns, respectively. It is evident that this structure can not be very stable owing to the strong lattice strains in the core region. Thus a dissociation of the core is likely. This is proven by the HRTEM image (Fig. 1) which shows a climb-dissociated dislocation core structure. The pairs of partial dislocations are arranged

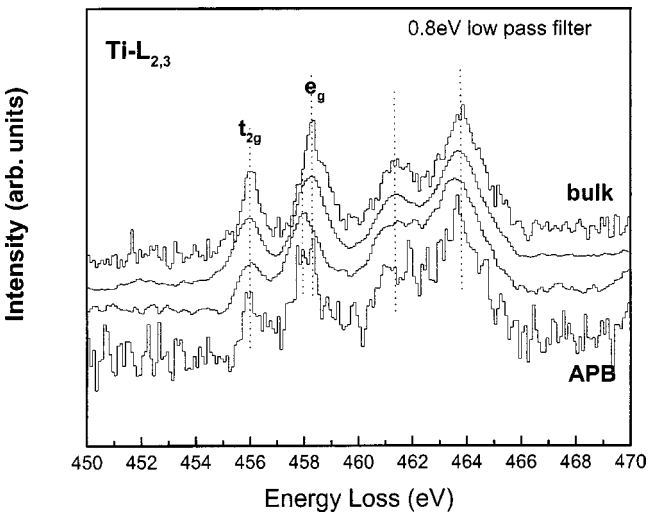

FIG. 5. Enlargements of the Ti-$L_{2,3}$ edge spectra extracted from the EELS map, one from the APB area and the other from the surrounding bulk region. Also shown are the same spectra after smoothing with a 0.8 eV low pass filter.

in the grain boundary with almost identical spacing. Based on this image (in the bulk white spots represent Ti or Sr columns), a possible atomic model of the dissociated dislocation was established which is shown in Fig. 6(b). Whereas the lower partial is terminated by Ti/O atom columns, the upper partial is terminated by Sr/O columns. The APB between the partials is visible by the disregistry of the Ti/O-Sr/O column sequence along the [110] direction. The APB area is shaded in Fig. 6(b). It should be pointed out that the shown atomic model of the dislocation core is not an energetically minimized structure. This would require further atom relaxations calculated from atomistic simulations.

The APB energy can be calculated from the separation of the partial dislocations shown in Fig. 1. This is true if the separation has reached its equilibrium value which is determined by the repulsive force of the partials and the attractive force due to the APB. In the present case we have to consider that climb was involved in the dissociation. Normally, point defects are necessary to allow dislocations to climb. In the case of partial dislocations this is not necessarily the case. In the present case the climb can be achieved by simply transferring atoms from the right-hand partial to the left-hand partial. This requires atom transport only over a few nanometers, which is easily possible under the diffusion-bonding conditions even for the heavy cations. We therefore conclude that the attainment of the equilibrium separation is not limited by diffusional processes. However, it may well be limited by the proximity of the dislocations within the GB. It is presently not clear whether this is the case or not. From the observed separations we can at least estimate an upper limit for the (110) APB energy. Because $SrTiO_3$ is almost perfectly elastically isotropic the (110) APB energy can be easily calculated.[28] We obtain as an upper limit of the (110) APB energy a value of $(720 \pm 280)\ \mathrm{mJ/m^2}$. For the {110} plane, Matsunaga and Saka[29] reported an APB value of $136 \pm 15\ \mathrm{mJ/m^2}$ for $a/2\langle 110\rangle$ glide. This is much lower than our value and could indicate that the partials observed by us

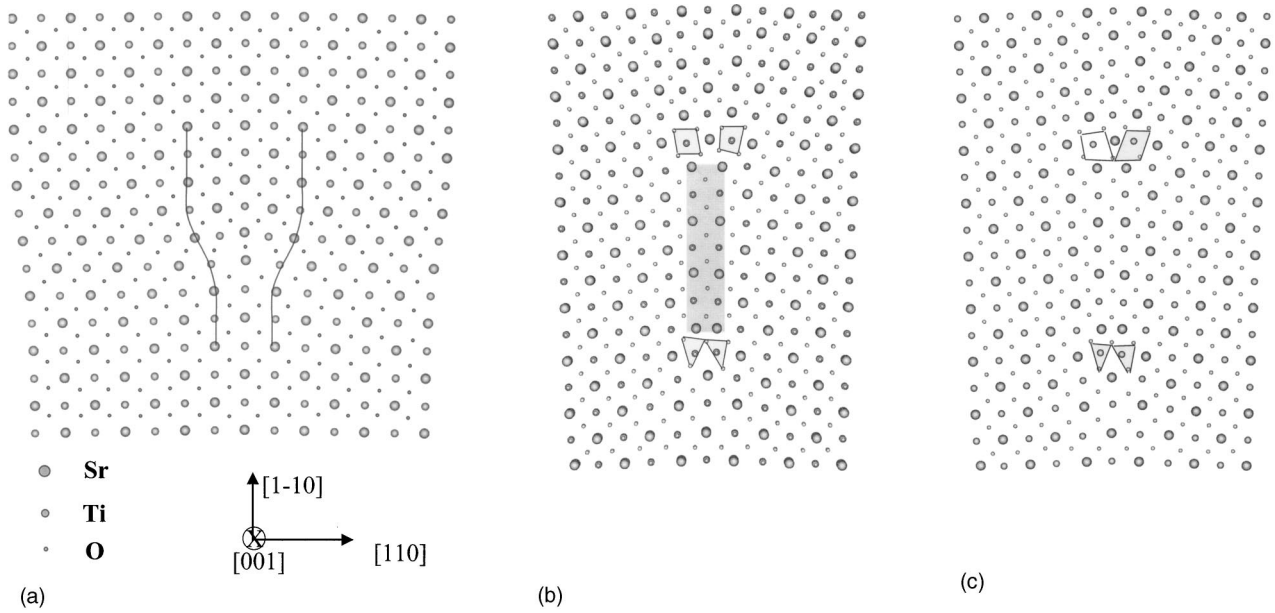

FIG. 6. Atomistic model for the $a\langle 110\rangle$ dislocation core. (a) Perfect $a\langle 110\rangle$ edge dislocations without dissociation. (b) After climb dissociation; the shaded area is APB. (c) After removing one oxygen atom column from the structure shown in (b).

have not reached the equilibrium separation. Mao and Knowles[30] found for $a/2\langle 110\rangle$ *climb* on the {100} plane an APB energy of 245 ± 30 mJ/m^2 and for $a/2\langle 110\rangle$ *glide* on the {100} plane 145 ± 15 mJ/m^2.

In order to improve the correspondence with our EELS results we further modified the structure shown in Fig. 6(b). Basically we removed one oxygen atom column in order to obtain a good fit to the measured Ti/O ratio [Fig. 6(c)]. This core structure indicates that the two Ti-O octahedra share a corner compared with Fig. 6(b). This leads to a better correspondence with the experimentally determined Ti/O and Sr/Ti ratios, especially from the mapping measurement. The core structure as proposed in Fig. 6(c) exhibits the following features.

(1) Owing to the termination of the inserted planes the upper partial core can be assigned as a Sr-rich core, the lower one as a Ti-rich core.

(2) By counting the atoms in Fig. 6(c) with the almost same area as in the mapping measurements (about 0.6×0.6 nm^2) we find that in the Ti-rich core the Ti/O ratio is increased by 10% while the Sr/Ti ratio is decreased by about 20% compared with the bulk value, and in the Sr-rich core the Sr/Ti ratio is increased by about 25% while the Ti/O ratio is slightly increased compared with the bulk.

This means that both cores show an increased Ti/O ratio which is in good agreement with the experiment. It should be noted that by the removal of one oxygen column both cores become positively charged. This leads to a repulsive force between the partial dislocations. However, for separations exceeding 0.1 nm (which is well below the observed 2.48 nm) this Coulomb force is negligible as compared to the elastic forces acting on the partials.

The correlation of the Ti-$L_{2,3}$ and O-K near-edge structures with structural features in $SrTiO_3$ was reviewed in a previous paper.[22] The ELNES obtained from the partial dislocations exhibits clear differences compared to the bulk. The increased Ti/O intensity ratio in the partial core was also found in the $a\langle 100\rangle$ dislocation core[22] and at other GBs in $SrTiO_3$.[31–34] This seems to be a general feature of crystal defects in $SrTiO_3$. Compared to the bulk, the e_g/t_{2g} ratio is increased in the $a[100]$ core, whereas it is decreased in the $a/2[110]$ core. The magnitude of this effect is much more pronounced in the $a\langle 110\rangle$ partial cores where both peaks are of similar height. In Fig. 4(b), both peaks have even become one. According to van der Laan and Kirkman[35] the e_g/t_{2g} ratio increases by a reduction of the crystal field, i.e., in the partial cores the crystal field appears to be strongly increased. However, the reduced ligand field splitting is indicative of a reduced crystal field. It remains an open question at the moment how these changes in the Ti-$L_{2,3}$ ELNES are to be interpreted. A possible approach is to use real space band structure calculations based on structures proposed in Fig. 6.

From the area measurement and mapping another obvious feature is that the intensity ratio of L_3/L_2 in the cores is increased. From the literature it is not clear whether this ratio changes by a change in the oxidation state. Whereas Leapman *et al.*[36] found the same ratio for TiO_2 and metallic Ti, Otten *et al.*[37] and Waddington *et al.*[38] found a decrease of the L_3/L_2 ratio with the oxidation state. If the latter was true, our experiments would suggest a reduced oxidation state in the partial cores. This further supports the removal of oxygen atoms from the core [Figs. 6(b) and 6(c)].

Similar to the dislocation cores, a reduction of the ligand-field splitting by 0.3 eV is also present in the APB. From the atomistic model [Fig. 6(b)] it can be seen that in the APB area the oxygen coordination of Ti does not change. However, the separation of nearest Ti atoms is reduced from a to $a/\sqrt{2}$ in the APB, which reduces the crystal field imposed by the oxygen nearest neighbors.

V. CONCLUSION

The atomistic and electronic structure as well as the chemistry in the core of $a/2\langle 110\rangle$ partial dislocations in $SrTiO_3$ were studied by HRTEM and EELS. Well-pronounced differences in the Sr/Ti ratio were detected between the two partials. Generally, a reduced crystal field around the Ti atoms as well as an increased Ti/O ratio was found in both partials. These results can be brought to a good correspondence with atomistic models if oxygen atoms are removed from the core region. It is presently not clear if the proposed structural models can explain the changes of the e_g/t_{2g} and L_2/L_3 ratios in the core regions. This will require theoretical calculations of ELNES.

In comparison to the present results of the $a\langle 110\rangle\{110\}$ dislocation, the $a\langle 100\rangle\{100\}$ dislocation studied previously[22] was found to exhibit a rather compact core structure. This certainly has to do with the shorter Burgers vector of the $a[100]$ dislocation. But it may also be affected by the different slip planes of the two dislocations which result in different free energies of the APB's separating the partials. This would suggest a rather high APB free energy on the {100} plane as compared to that of the {110} plane; however, this is rather speculative. Apart from a dissociation on the slip plane one could imagine that the $a\langle 100\rangle\{100\}$ dislocation could also dissociate by climb. However, from simple structural reasons this would require the long-range migration of point defects (in contrast to the $a\langle 110\rangle\{110\}$ dislocation, where only short-range migration is required; see Sec. IV) which for Ti and Sr atoms is unlikely to occur.

The climb dissociated structure of the $a\langle 110\rangle\{110\}$ dislocation may have important consequences on the plastic behavior of $SrTiO_3$.[39,40] It was shown that, under compression along the $\langle 100\rangle$ axis, plasticity at low and high temperatures is dominated by $\langle 110\rangle\{110\}$ slip, but with a very strong yield stress anomaly resulting in higher flow stresses at elevated temperatures. We assigned this to different dislocation core structures at low and high temperatures.[40] It is clear that the movement of a climb-dissociated dislocation is considerably hindered by the presence of the APB on a nonslip plane. Bretheau *et al.*[41] discussed various mechanisms for the movement of climb-dissociated dislocations. All of them require high thermal activation. Since our bicrystals were diffusion bonded at high temperatures, we assume that the climb-dissociated core structure corresponds to the high-temperature configuration of the dislocation core.

ACKNOWLEDGMENTS

One of the authors (Z.L.Z.) is grateful for financial support from the Max-Planck Society. We also thank Maria Sycha for the excellent TEM specimen preparation. We thank Dr. C. Elsässer, Dr. C. Scheu, and Dr. K. van Benthem for helpful discussions.

[1] M. Cardona, Phys. Rev. **140**, A651 (1965).
[2] I. Tanaka, T. Nakajima, J. Kawai, H. Adachi, H. Gu, and M. Rühle, Philos. Mag. Lett. **75**, 21 (1997).
[3] S. Hutt, S. Köstlmeier, and C. Elsässer, J. Phys.: Condens. Matter **13**, 3949 (2001).
[4] S.-D. Mo, W. Y. Ching, M. F. Chisholm, and G. Duscher, Phys. Rev. B **60**, 2416 (1999).
[5] V. Ravikumar and V. P. Dravid, Ultramicroscopy **52**, 557 (1993).
[6] V. P. Dravid and V. Ravikumar, Interface Sci. **8**, 177 (2000).
[7] X. Pan, H. Gu, S. Stemmer, and M. Rühle, Mater. Sci. Forum **207**, 421 (1996).
[8] M. M. McGibbon, N. D. Browning, M. F. Chisholm, A. J. McGibbon, S. J. Pennycook, V. Ravikumar, and V. P. Dravid, Science **266**, 102 (1994).
[9] N. D. Browning, S. J. Pennycook, M. F. Chisholm, M. M. McGibbon, and A. J. McGibbon, Interface Sci. **2**, 397 (1995).
[10] N. D. Browning and S. J. Pennycook, J. Phys. D **29**, 1779 (1996).
[11] O. Kienzle and F. Ernst, J. Am. Ceram. Soc. **80**, 1639 (1997).
[12] O. Kienzle, F. Ernst, and G. Möbus, J. Microsc. **190**, 144 (1998).
[13] O. Kienzle, M. Exner, and F. Ernst, Phys. Status Solidi A **166**, 57 (1998).
[14] R. Feidenhans'l, A. Kazimirov, D. M. Smilgies, Q. Jiang, and J. Zegenhagen, Philos. Mag. Lett. **78**, 51 (1998).
[15] Y.-M. Chiang and T. Takagi, J. Am. Ceram. Soc. **73**, 3286 (1990).
[16] S. B. Desu and D. A. Payne, J. Am. Ceram. Soc. **73**, 3391 (1990).
[17] R. Brydson, H. Sauer, W. Engel, and F. Hofer, J. Phys.: Condens. Matter **4**, 3429 (1992).
[18] N. D. Browning, H. O. Moltaji, and J. P. Buban, Phys. Rev. B **58**, 8289 (1998).
[19] P. E. Batson, Phys. Rev. Lett. **83**, 4409 (1999).
[20] N. D. Browning, I. Arslan, Y. Ito, E. M. James, R. F. Klie, P. Moeck, T. Topuria, and Y. Xin, J. Electron. Microsc. **50**, 205 (2001).
[21] R. A. de Souza, J. Fleig, J. Maier, O. Kienzle, Z. L. Zhang, W. Sigle, and M. Rühle (unpublished).
[22] Z. L. Zhang, W. Sigle, and M. Rühle, Phys. Rev. B **66**, 094108 (2002).
[23] W. Kurtz, Z. Metallkd. **93**, 432 (2002).
[24] H. F. Fischmeister, G. Elßner, B. Gibbesch, K.-H. Kadow, F. Kawa, D. Korn, W. Mader, and M. Turwitt, Rev. Sci. Instrum. **64**, 234 (1993).
[25] R. F. Egerton, *Electron Energy Loss Spectroscopy in the Electron Microscope*, 2nd ed. (Plenum, New York, 1996).
[26] The Ti-$L_{2,3}$ edge originates from dipole-allowed excitations of electrons from the inner $2p_{3/2}$ (L_3 edge) and $2p_{1/2}$ levels (L_2 edge) to the unoccupied $3d$ band. The resulting two white lines are doubled by the action of the Coulomb field imposed by the surrounding O atoms. A perfect octahedral ligand field causes the five degenerate d states in the conduction band to split into the twofold e_g orbitals which are directed at the ligands and the threefold t_{2g} orbitals which are directed between the ligands.
[27] D. H. Pearson, C. C. Ahn, and B. Fultz, Phys. Rev. B **47**, 8471 (1993).
[28] J. P. Hirth and J. Lothe, *Theory of Dislocations* (Wiley, New York, 1968).
[29] T. Matsunaga and H. Saka, Philos. Mag. Lett. **80**, 597 (2000).
[30] Z. Mao and K. M. Knowles, Philos. Mag. **73**, 699 (1996).

[31] S. Stemmer, S. K. Streiffer, N. D. Browning, C. Basceri, and A. I. Kingon, Interface Sci. **8**, 209 (2000).
[32] G. Duscher, J. P. Buban, N. D. Browning, M. F. Chisholm, and S. J. Pennycook, Interface Sci. **8**, 199 (2000).
[33] K. van Benthem, R. H. French, W. Sigle, C. Elsässer, and M. Rühle, Ultramicroscopy **86**, 303 (2001).
[34] M. Y. Kim, G. Duscher, N. D. Browning, K. Sohlberg, S. T. Pantelides, and S. J. Pennycook, Phys. Rev. Lett. **86**, 4056 (2001).
[35] G. van der Laan and I. W. Kirkman, J. Phys.: Condens. Matter **4**, 4189 (1992).
[36] R. D. Leapman, L. A. Grunes, and P. L. Fejes, Phys. Rev. B **26**, 614 (1982).
[37] M. T. Otten, B. Miner, J. H. Rask, and P. R. Buseck, Ultramicroscopy **18**, 285 (1985).
[38] W. G. Waddington, P. Rez, I. P. Grant, and C. J. Humphreys, Phys. Rev. B **34**, 1467 (1986).
[39] D. Brunner, S. Taeri-Baghbadrani, W. Sigle, and M. Rühle, J. Am. Ceram. Soc. **84**, 1161 (2001).
[40] P. Gumbsch, S. Taeri-Baghbadrani, D. Brunner, W. Sigle, and M. Rühle, Phys. Rev. Lett. **87**, 085505 (2001).
[41] T. Bretheau, J. Castaing, J. Rabier, and P. Veyssière, Adv. Phys. **28**, 835 (1979).